Electronic Supplementary Information (ESI)

On the physicochemical origin of the nanoscale friction: the polarizability and electronegativity relationship tailoring nanotribology

Leonardo M. Leidens[a], Marcelo E. H. Maia da Costa[b], Neileth S. Figueroa[b], Rodrigo A. Barbieri[c], Fernando Alvarez[d], Alexandre F. Michels[a] and Carlos A. Figueroa[a,e*]

[a]*Programa de Pós-Graduação em Engenharia e Ciência dos Materiais (PPGMAT), University of Caxias do Sul (UCS) – 95070-560, Caxias do Sul – RS, Brazil*

[b]*Physics Department, Pontifical Catholic University of Rio de Janeiro (PUC-RIO) – 22453-900, Rio de Janeiro – RJ, Brazil*

[c]*Central Laboratory of Microscopy (LCMIC), University of Caxias do Sul (UCS) – 95070-560, Caxias do Sul – RS, Brazil*

[d]*Institute of Physics "Gleb Wataghin", Campinas State University (UNICAMP) – 13083-970, Campinas – SP, Brazil*

[e]*Plasmar Tecnologia Ltda – 95030-775, Caxias do Sul – RS, Brazil*

1. X-ray photoelectron spectroscopy (XPS) – complete spectra

Figure S1 shows the complete XPS spectra of the current set of amorphous carbon samples with indication of the region for F 1s, O 1s, N 1 s and C 1s core level bands. The progressive increase in fluorine intensity with the increase of CF_4 proportion in the deposition atmosphere is evident.

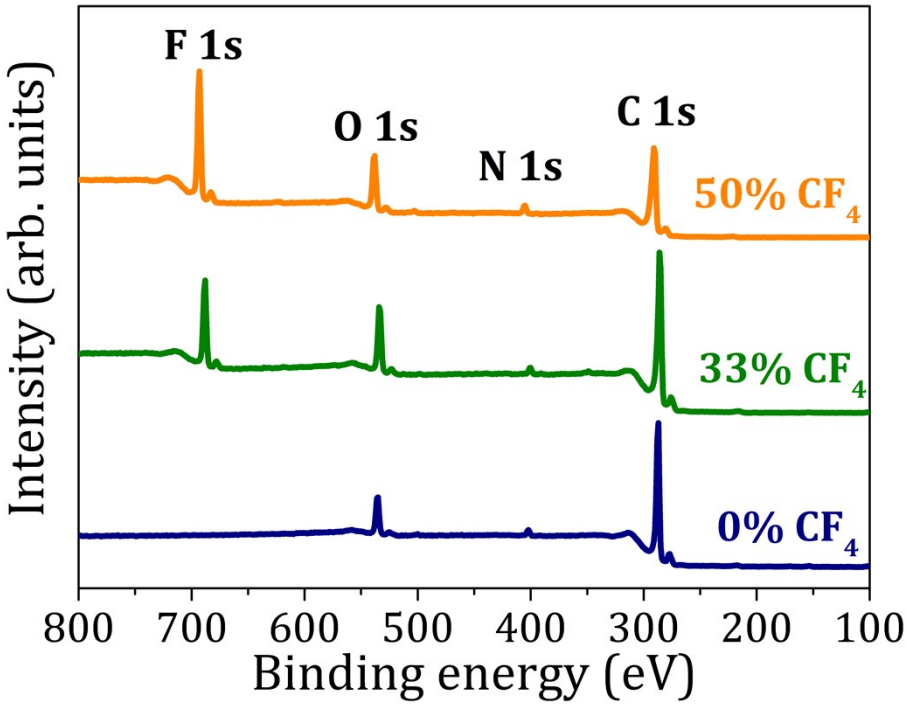

Figure S1 – Complete XPS spectra of the current set of samples with indication of the region of F 1s, O 1s, N 1 s and C 1s core levels. One can note the progressive increase in fluorine intensity with the increase of CF_4 proportion in the deposition atmosphere

2. Linear fitting of hydrogen content (at. %) and density with F/C ratio for amorphous carbon sister thin films

In order to estimate the hydrogen content of the current films, it was possible to compare the atomic ratio between F and C (F/C) from the current and previous sister

samples, published elsewhere[1], since F increases at the same time of H and C decrease for previous samples. Moreover, the same correlation was used to estimate the atomic density of the materials. Figures S2 and S3 shows, respectively, the data for H (at. %) from [1] and the linear fitting. Both the hydrogen at. % and atomic density of the current samples were calculated using the F/C ratio and the linear fitted equation obtained for the previous samples. The results were plotted as crosses in the same graph to better illustrate the similarity and, as shown, they are within the linear range of the sister samples, permitting the estimation without further extrapolation.

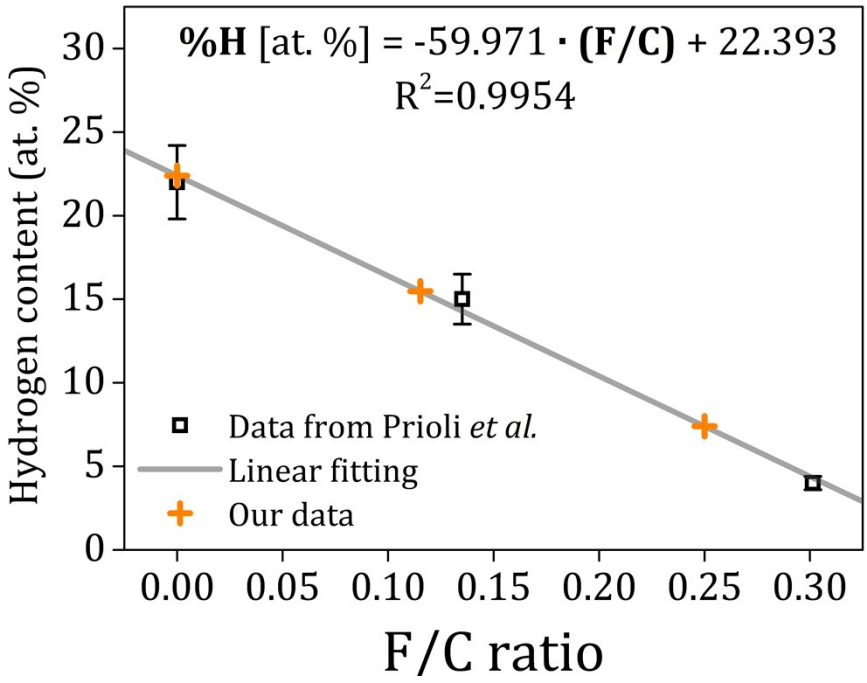

Figure S2 – Linear fitting of the relationship between F/C ratio and hydrogen atomic content (at. %) from previously published[1] amorphous carbon samples. The crosses represent the F/C data for the current samples.

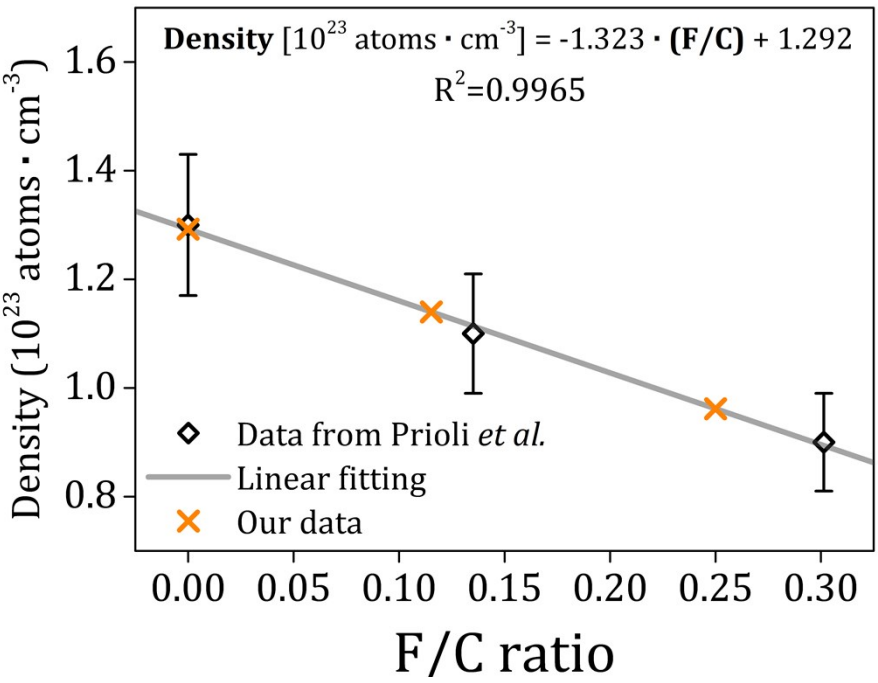

Figure S3 – Linear fitting of the relationship between F/C ratio and the atomic density from previously published[1] amorphous carbon samples. The crosses represent the F/C data for the current samples.

3. Raman spectroscopy – background correction and deconvolution (curve fitting)

Figures S4, S5 and S6 show the deconvolution of Raman spectra for the three carbon-based films in order to measure the band intensities ratio (I_D/I_G) and the position of the G band. The measurements were conducted after background correction and Gaussian fitting (two bands corresponding to D- and G-band regions).

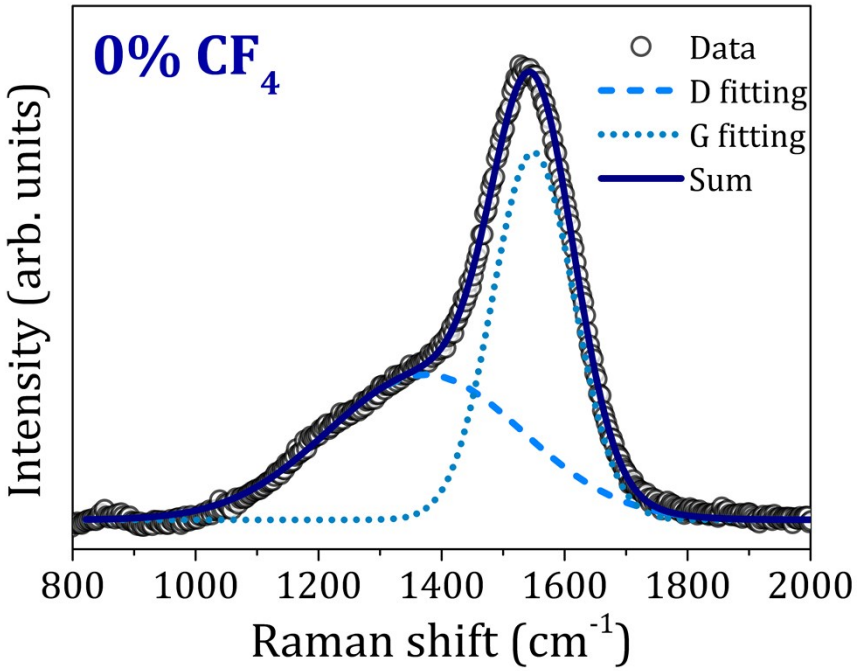

Figure S4 - Raman spectrum of the samples deposited with 100% C_2H_2 gas precursor. The deconvolution was performed after background correction (elimination of luminescence effect) with two gaussian curves in the region of D- and G-bands.

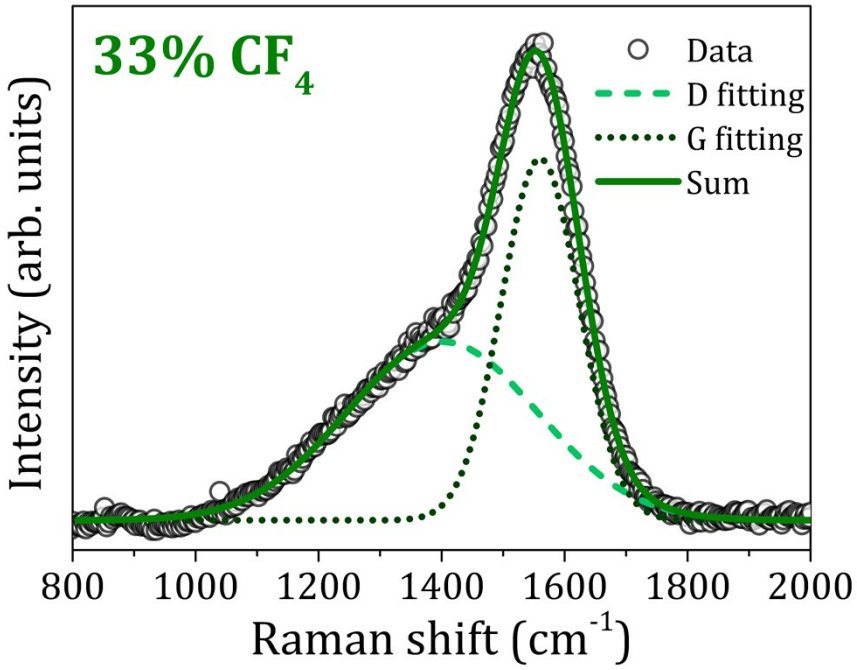

Figure S5 - Raman spectrum of the samples deposited with 33% CF_4 and 67% C_2H_2 gas mixture. The deconvolution was performed after background correction (elimination of luminescence effect) with two gaussian curves in the region of D- and G-bands.

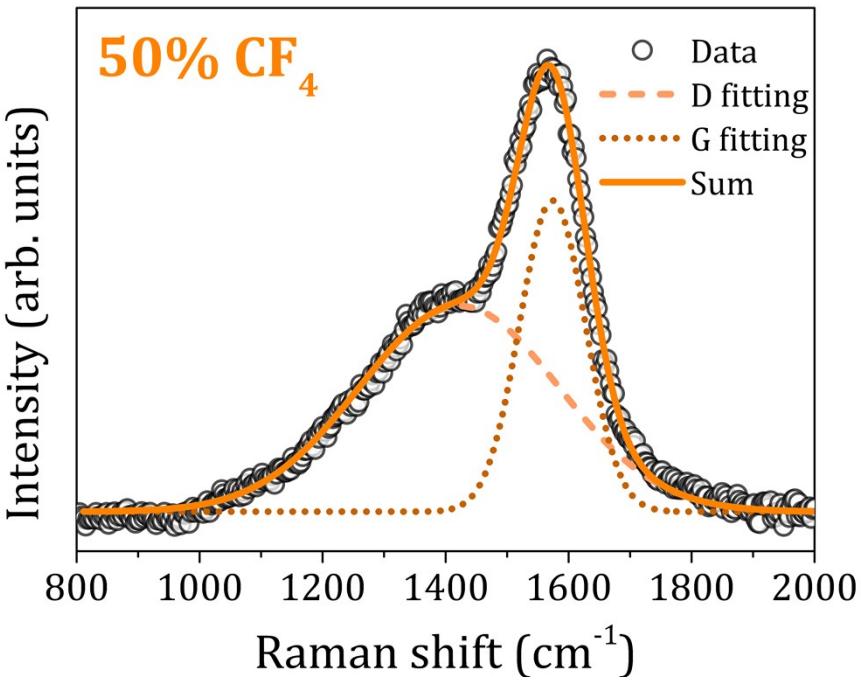

Figure S6 - Raman spectrum of the samples deposited with 50% CF_4 and 50% C_2H_2 gas mixture. The deconvolution was performed after background correction (elimination of luminescence effect) with two gaussian curves in the region of D- and G-bands.

4. Lateral force microscopy (LFM) experimental details

Bidirectional sliding tests were performed by lateral force microscopy (LFM) using an atomic force microscope (AFM - SPM-9700 – Shimadzu) equipped with a silicon tip (PPP-LFMR, Nanosensors) with nominal ending radius < 10 nm. The tip is mounted on a rectangular shaped cantilever (with Al coating deposition to enhance laser reflection). Temperature and relative humidity were controlled and kept at 18ºC ± 2 and 49% ± 1, respectively, during the experiments. In order to analyze quantitatively the friction force (originally a signal in volts units regarding the lateral deflection of the cantilever) obtained in the equipment, it was necessary to previously calibrate the tip. Since the cantilever used is rectangular it is possible to perform a geometric calibration, used in different published works[1,2] and finally summarized by Gnecco and collaborators[3]. The

obtained calibration factor is in good agreement with other methods, when used the same tip and similar conditions as expressed in a review paper[4]. The images were obtained (size of 1 x 1 μm) with a resolution of 512 x 512 pixels at a constant velocity. The normal load was varied in order to assess the friction behavior in function of the applied load. Data was, finally, analyzed using Gwyddion, an open-source software[5] available online at http://gwyddion.net/.

5. Linear fitting of friction experimental results

The experimental results to each sample with different normal load are presented in Figures S7, S8 and S9. Since a clear linear behavior is observed, linear curves were fitted in each graph. Therefore, the fitted equation, deviation and respective R^2 are also show in the figures.

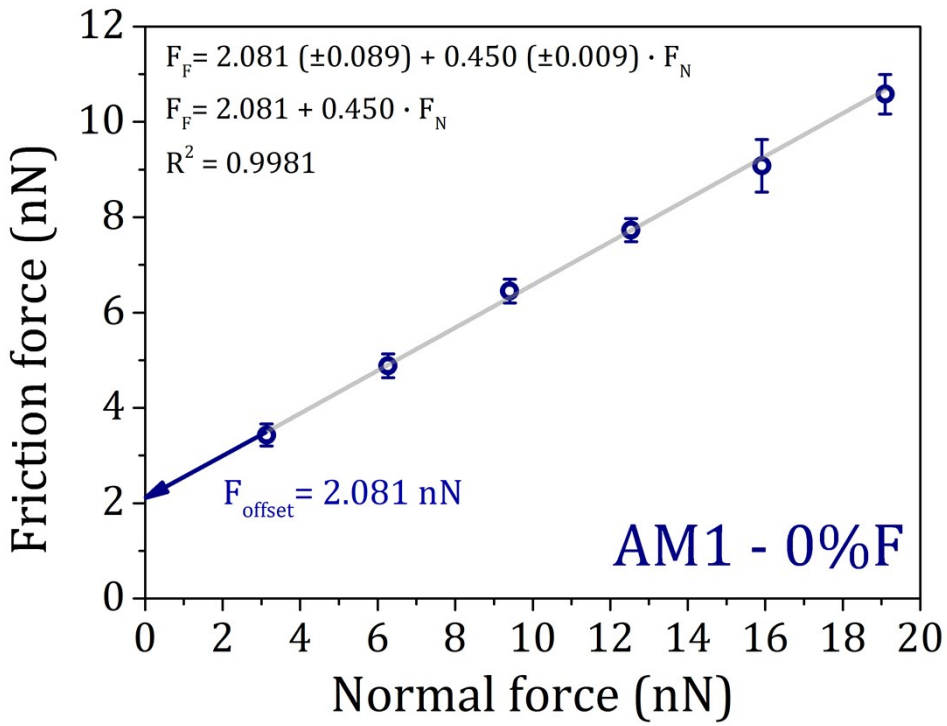

Figure S7 - Friction force in function of the normal load applied during the experiments in sample 0%F (without fluorine). The linear correlation was extrapolated to verify the offset friction force used in the discussion.

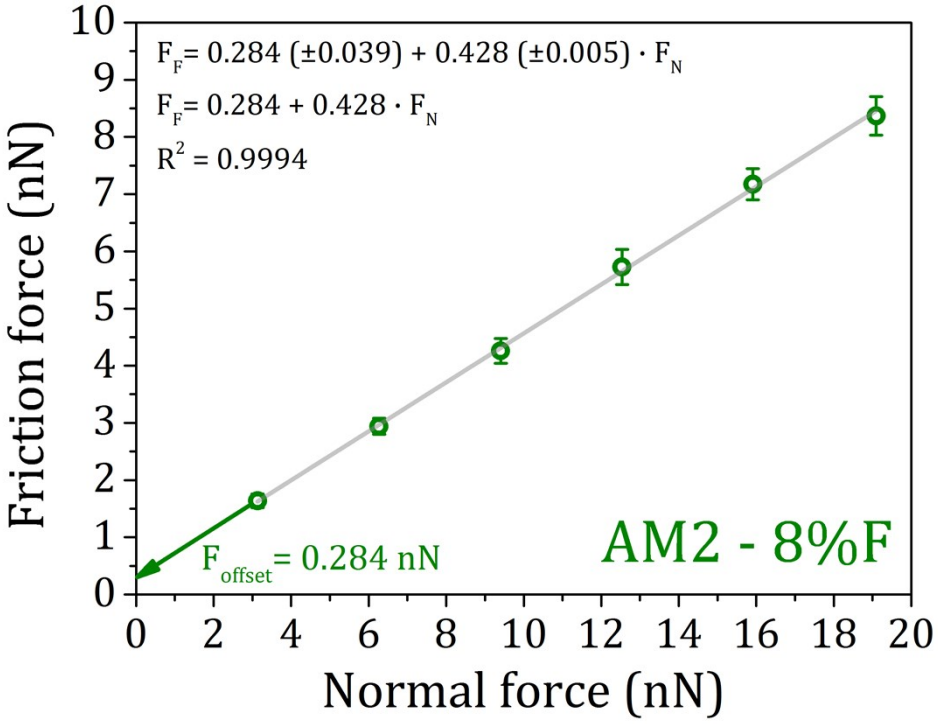

Figure S8 - Friction force in function of the normal load applied during the experiments in sample 8%F. The linear correlation was extrapolated to verify the offset friction force used in the discussion.

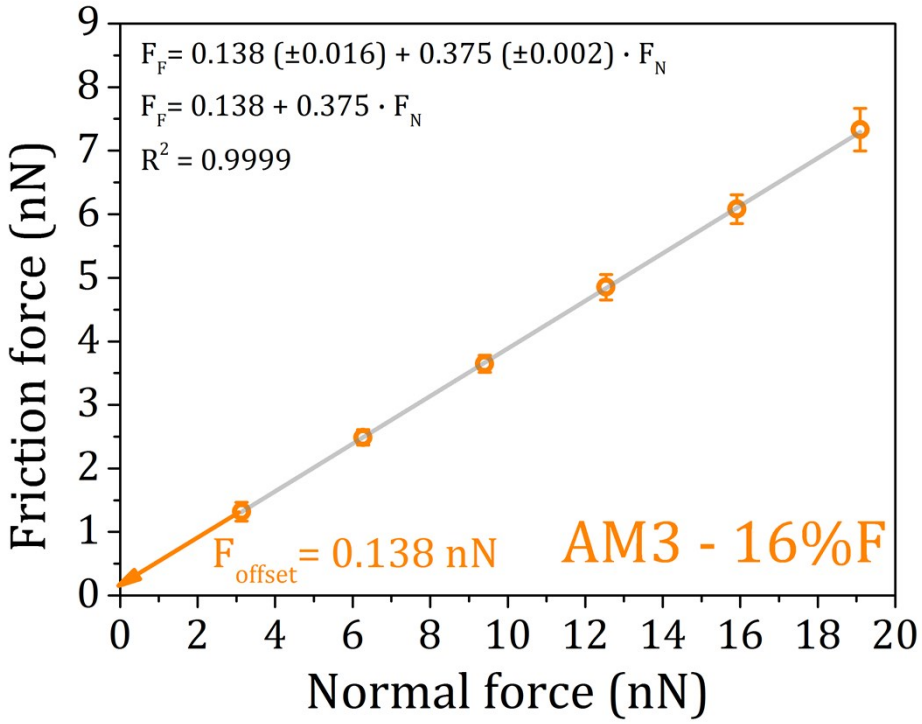

Figure S9 - Friction force in function of the normal load applied during the experiments in sample 16%F. The linear correlation was extrapolated to verify the offset friction force used in the discussion.

6. Roughness

Roughness measurements were also performed by using the Gwyddion software's tools and the topographical images obtained during lateral force sliding experiments. Ra (arithmetic average of the absolute values of the profile height deviations from the mean line) and RMS (root mean square average of the profile height deviations from the mean line) parameters were, finally, calculated for each sample. In Table S1, the roughness parameters are presented. The reported error corresponds to the standard deviation of several linear measurements. One can note that, although minor differences in roughness, within the experimental error, all the values are very close, indicating that the roughness, both Ra and RMS, of the films studied in this work may not play a crucial role in the reported friction results.

Table S1 – Roughness parameters (Ra and RMS) of the set of samples evaluated

Sample	Ra (nm)	RMS (nm)
0%F	4.15 ± 0.54	5.26 ± 0.81
8%F	4.79 ± 0.58	6.02 ± 0.67
16%F	4.41 ± 0.42	5.54 ± 0.61

7. Comparison between samples with 8%F and 16%F

Figure S10 shows the ratio for both experimental and theoretical frictional forces, between a-C:F:H with 16 at. %F / a-C:F:H with 8 at. %F. As already discussed in the manuscript, experiment results and the proposed model present good agreement and, therefore, we infer that the friction behavior at nanoscale and elastic regime is dependent of the physical-chemical properties of the interacting surfaces.

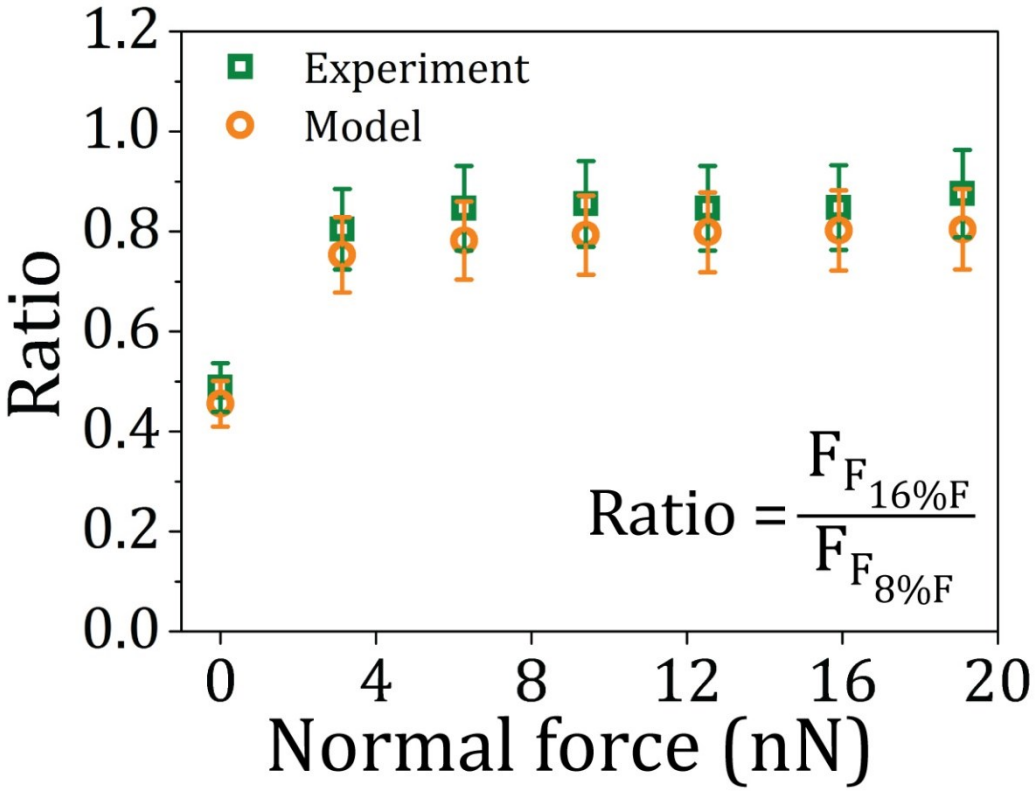

Figure S100 - Comparison of experimental and theoretical friction forces as a function of the normal load with the ratio between fluorinated samples

8. Physical-chemical damping constant (η_{PC}) calculation

Table S2 presents the parameters used to determine the physical-chemical damping constant. The polarizabilities were obtained in a recently published paper[9] that calculated such parameter by means of other periodic descriptors. Although the different method, the results agree with other calculations, compiled in a recent review[10]. The polarizabilities are originally in atomic units (a.u.) and, in order to perform the calculations were converted using the relation 1 a.u. = 0,14818471 Å³.

Table S2 – Polarizability for each chemical element present in the sample and/or the tip

Chemical element	Polarizability (α) [Å³. atom^{-1}]
C	1.935
H	0.667
F	0.550
Si	5.468

A weighted sum of the atomic fractions presented in the manuscript multiplied by the property in question was used, as presented in Equation (I). For the tip, the properties of silicon were used, considering that the tip consists of pure silicon.

$$\alpha_{sample} = (f_C \cdot \alpha_C) + (f_H \cdot \alpha_H) + (f_F \cdot \alpha_F) \#(I)$$

With f_i being the atomic fraction of chemical element i.

Finally, it was possible to obtain the physical-chemical damping constant with equation (II) and the results are presented in Table S3.

$$\eta_{PC} = [\alpha_{sample} \cdot \rho_{sample}] \cdot [\alpha_{tip} \cdot \rho_{tip}] \#(II)$$

Table S3 – Results for the sample and tip term separatedly and the final damping constant used in comparasion.

Sample	η_{PC} (sample)	η_{PC} (tip)	η_{PC} (total)
0%F	0.210	0.273	0.057
8%F	0.178	0.273	0.049
16%F	0.145	0.273	0.040

The physical-chemical damping constant is a dimensionless number. However, with the units used and showed in Table S2, a 10^{-2} factor appears as follows (and it is already considered in Table S3):

$$\eta_{PC} = [\alpha_{sample} \cdot \rho_{sample}] \cdot [\alpha_{tip} \cdot \rho_{tip}] \#(III)$$

$$\eta_{PC} = \left[\frac{Å^3}{atom}\right]^2 \cdot \left[\frac{10^{23} atoms}{cm^3}\right]^2 \cdot \left[\frac{10^{-24}\, cm^3}{Å^3}\right]^2 = 10^{-2} \#(IV)$$

9. Friction offset correction

In order to use the offset in frictional force in the theoretical expression, a correction is necessary. The procedure consists of divide the offset force by the friction coefficient obtained in linear fitting, since the physical-chemical damping constant is a contribution to the coefficient of friction and already considered in the frictional offset. In this way, it was possible to sum the normal contributions from both inherent attractive contact interaction and the nominal, applied in the tip during experiments. Table S4 presents the results.

Table S4 – Friction offset and coefficient of friction (μ) of the three samples as well as the F_{offset} correction to inclusion on theoretical calculations.

Sample	F_{offset} (nN)	μ	Normal contribution [(F_{offset})/μ] (nN)
0%F	2.0806	0.4498	4.6256
8%F	0.2835	0.4280	0.6624
16%F	0.1384	0.3745	0.3696

References

1 Y. B. Guo, D. G. Wang and S. W. Zhang, Adhesion and friction of nanoparticles/polyelectrolyte multilayer films by AFM and micro-tribometer, *Tribol. Int.*, 2011, **44**, 906–915.

2 Q. Liu and Z. Kang, Preparation and micro-tribological property of hydrophobic organic films on the surface of Mg-Mn-Ce magnesium alloy, *Prog. Org. Coatings*, 2015, **84**, 42–49.

3 E. Gnecco, R. Pawlak, M. Kisiel, T. Glatzel and E. Meyer, in *Nanotribology and Nanomechanics: An Introduction: Fourth Edition*, 2017.

4 B. C. Tran Khac and K. H. Chung, Quantitative assessment of contact and non-contact lateral force calibration methods for atomic force microscopy, *Ultramicroscopy*, 2016, **161**, 41–50.

5 D. Nečas and P. Klapetek, *Cent. Eur. J. Phys.*, 2012, 10, 181–188.

6 R. Prioli, L. G. Jacobsohn, M. E. H. Maia da Costa and F. L. Freire, Nanotribological properties of amorphous carbon-fluorine films, *Tribol. Lett.*, 2003, **15**, 177–180.

7 E. Riedo, F. Lévy and H. Brune, Kinetics of capillary condensation in nanoscopic sliding friction, *Phys. Rev. Lett.*, 2002, **88**, 1855051–1855054.

8 E. Gnecco, R. Bennewitz, T. Gyalog, C. Loppacher, M. Bammerlin, E. Meyer and H. J. Güntherodt, Velocity dependence of atomic friction, *Phys. Rev. Lett.*, 2000, **84**, 1172–1175.

9 H. Tandon, T. Chakraborty and V. Suhag, A new scale of atomic static dipole polarizability invoking other periodic descriptors, *J. Math. Chem.*, 2019, **57**, 2142–2153.

10 P. Schwerdtfeger and J. K. Nagle, 2018 Table of static dipole polarizabilities of the neutral elements in the periodic table*, *Mol. Phys.*, 2019, **117**, 1200–1225.